

## Electronic Supplementary Information to:

### Ti substrate grain dependent C/TiO<sub>2</sub> composites through carbothermal treatment of anodic TiO<sub>2</sub>

*Celine Rüdiger<sup>a,b\*</sup>, Marco Favaro<sup>c</sup>, Carlos Valero-Vidal<sup>b</sup>, Laura Calvillo<sup>c</sup>, Nathalie Bozzolo<sup>d</sup>, Suzanne Jacomet<sup>d</sup>, Clivia Hejny<sup>e</sup>, Luca Gregoratti<sup>f</sup>, Matteo Amati<sup>f</sup>, Stefano Agnoli<sup>c</sup>, Gaetano Granozzi<sup>c</sup>, Julia Kunze-Liebhäuser<sup>b\*</sup>*

<sup>a</sup> Physik-Department, Technische Universität München, James-Franck-Str. 1, 85748 Garching, Germany.

<sup>b</sup> Institut für Physikalische Chemie, Leopold-Franzens-Universität Innsbruck, Innrain 52c, 6020 Innsbruck, Austria.

<sup>c</sup> Dipartimento di Scienze Chimiche, Università di Padova, Via Marzolo 1, 35131 Padova, Italy.

<sup>d</sup> MINES ParisTech, PSL - Research University, CEMEF - Centre de Mise en Forme des Matériaux, CNRS UMR 7635, CS 10207 Rue Claude Daunesse 06904 Sophia Antipolis Cedex, France.

<sup>e</sup> Institut für Mineralogie und Petrographie, Leopold-Franzens-Universität Innsbruck, Innrain 52d, 6020 Innsbruck, Austria.

<sup>f</sup> Elettra – Sincrotrone Trieste SCpA, SS14-Km163.5 in Area Science Park, 34149 Trieste, Italy.

#### Supporting Experimental Details

##### *Preparation of C/TiO<sub>2</sub>*

The SPEM experiments required samples of 10 mm diameter, while samples of 15 mm diameter were used for the Raman experiments. Both types of samples were cut from the same precursor Ti rod. One side of each sample was mechanically polished using SiC grinding paper (grits: P1200, P2500 and P4000, Buehler, ITW Test & Measurement GmbH, Germany) and ethanol (technical grade). On the polished side, a disc of 8 mm (on the 10 mm samples) or 14 mm (on the 15 mm samples) was then electrochemically polished in a solution of 40% perchloric acid, methanol and butoxyethanol (all high purity) at  $-35\text{ °C} \pm 2\text{ °C}$  following a recipe of Arsov.<sup>1</sup> After placing the cross-scratch marker, the samples were cleaned in an ultrasonic bath with ethanol and with de-ionized (DI) water (Millipore-Milli-Q system, 18.2 MΩ).

For anodization a DC power supply (PE 1540, 40 V/3 A, Philips) and a multimeter (Votcraft Dual Display M-3650D) were employed.

For the carbothermal treatments, different reactor tubes and accordingly optimized gas flow rates (MKS mass flow controllers) were used: the larger samples were annealed in a reactor tube of 40 mm diameter with 200 sccm Ar, where 0.5 flow% of C<sub>2</sub>H<sub>2</sub> were added for 5 min after 60 min of pre-annealing. The small samples were annealed in a reactor tube of 15 mm diameter with 50 sccm Ar and addition of 0.2 flow% of C<sub>2</sub>H<sub>2</sub> for 10 min after 55 min of pre-annealing.

##### *Accuracy of EBSD measurements*

The accuracy of orientations determined by EBSD is typically in the range 0.5 - 1° when considered in the acquisition reference frame (which is linked to the microscope). When analyzed in the sample frame, additional uncertainty associated with the positioning of the sample in the SEM chamber has to be taken into account. In the present experiment, the actual accuracy of the angular values which will be given below can be considered to be in the range of 2 - 3°.

### *Additional Information on the micro-Raman spectroscopy experiments*

The laser power and acquisition time were adjusted starting from low values and increasing both until a good signal to noise ratio was achieved while no sample damage occurred. The exposure time for one spectrum was ~205 s. To compensate for instrumental drift in wavenumber or intensity axis, the spectrometer was re-calibrated several times during a set of measurements using a clean Si(111) surface, and if necessary the measured intensity was rescaled accordingly.

A qualitative value of the optical penetration depth,  $d$ , can be estimated with equation  $d = \lambda/2\pi k$ , where  $\lambda$  is the wavelength of the excitation source (532 nm) and  $k$  is the extinction coefficient (for anodic TiO<sub>2</sub>,  $k$  is taken from<sup>2</sup>). The penetration depth of graphite is about 50 nm<sup>3</sup> and that of anodic TiO<sub>2</sub> more than 4 μm. In the present study, we analyse a C/TiO<sub>2</sub> composite that consists of a few nm thick graphitic carbon overlayer (as estimated from SPEM) on a ~53 nm thick anodic TiO<sub>2</sub>. The Ti substrate is not Raman active due to its metallic nature; the corresponding free electrons undergo plasma-like oscillations under laser illumination, thus preventing lattice vibrations.

Therefore, Raman spectroscopy allows to extract structural and compositional information about the entire C/TiO<sub>2</sub> composite film. In particular, the Raman signal intensity depends on the present amount of detected species.

### *Additional Information on SPEM*

The SPEM microscope can operate in two modes: imaging and spectroscopy. In the first mode the sample surface is mapped by synchronized-scanning the sample with respect to the focused photon beam and collecting photoelectrons with a selected kinetic energy. The second mode is an XPS from a sub-micron spot.

Due to the layered structure of the C/TiO<sub>2</sub> composite, semi-quantitative elemental analysis is not applicable here. The determination of the material's stoichiometry from atomic sensitivity-corrected XPS peak areas is based on the assumption of a homogeneous mixture of the composing elements, which is not the case here.

## Supporting Results

### *Substrate grain orientations from the interference color of the anodic TiO<sub>2</sub> film*

There is no strong influence of the azimuthal orientation ( $\varphi_2$ ) of the Ti substrate on the interference colors of the anodic TiO<sub>2</sub> film. Therefore, without EBSD map, one cannot deduce this orientation angle only from the optical appearance of the oxide film.

Nevertheless, at least for some Ti substrate orientations, the anodic films on top of Ti grains with similar tilt angles  $\Phi$  but with very different azimuthal orientations ( $\varphi_2$ ) have slightly different interference colors. As can be seen in Figure 1 of the main paper, grain 19 ( $\Phi = 36.3^\circ$ ,  $\varphi_2 = 8.8^\circ$ ) appears darker than grain 11 ( $\Phi = 30^\circ$ ,  $\varphi_2 = 22.3^\circ$ ) although it exhibits a slightly larger tilt angle  $\Phi$ . The same holds for grain 17 ( $\Phi = 46.4^\circ$ ,  $\varphi_2 = 0.3^\circ$ ) compared to grain 15 ( $\Phi = 42.6^\circ$ ,  $\varphi_2 = 27^\circ$ ). This brings about an error for  $\Phi$ -values that are estimated only from the optical appearance of the oxide film. The accuracy of  $\Phi$  can be considered to be ~5°.

### *Substrate grain orientations from the optical appearance of TiO<sub>2</sub><sup>ref</sup> and C/TiO<sub>2</sub>:*

After the annealing at 550 °C, the optical appearance of the anodic TiO<sub>2</sub> film changes significantly. Figure S1 shows an optical micrograph of the reference TiO<sub>2</sub><sup>ref</sup>, produced by a thermal treatment without acetylene (C<sub>2</sub>H<sub>2</sub>). Its colors can be grouped according to the four defined ranges of the angle  $\Phi$  (see standard triangle). In addition, on ~Ti{2110} ( $\varphi_2 \sim 30^\circ$ ) oriented grains, TiO<sub>2</sub><sup>ref</sup> exhibits a dark red color (see grains no. 4, 7 and 12) that can be distinguished from all other grains with  $\Phi \geq \sim 50^\circ$ . On ~Ti{1010} ( $\varphi_2 \sim 0^\circ$ ) oriented grains, TiO<sub>2</sub><sup>ref</sup> appears dark blue. After the treatment of the anodic TiO<sub>2</sub> films with C<sub>2</sub>H<sub>2</sub>, their optical

appearance (see Figure S2) is identical to that observed after the annealing in Ar without  $C_2H_2$ . The change in apparent color can be attributed to color centers within the  $TiO_2$  film caused by oxygen vacancies that are generated during the annealing in reducing atmosphere (and in particular in presence of an interface with the Ti substrate).

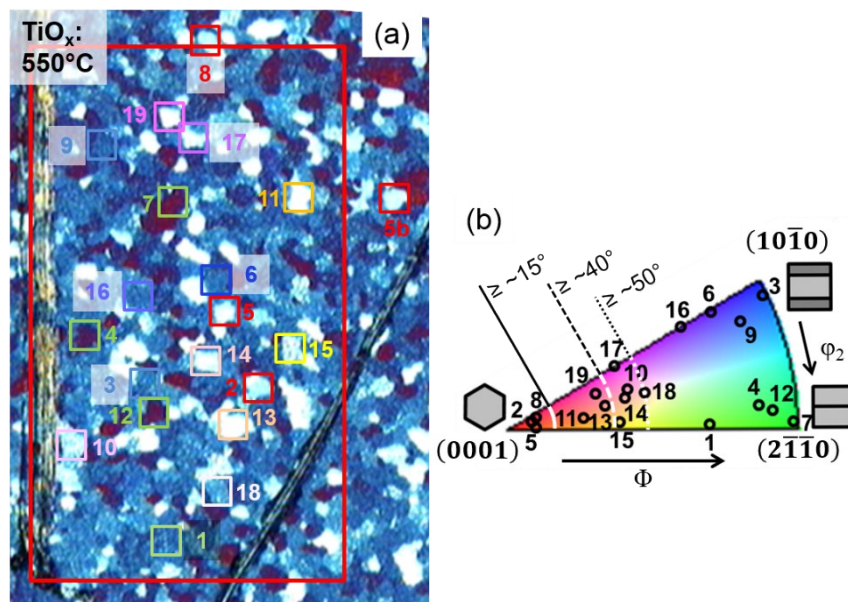


**Figure S1.** (a) Optical micrograph of anodic film of Figure 1 after thermal treatment in Ar for 1h at 550 °C ( $TiO_2^{ref}$ ); (b) standard triangle of EBSD map (zone within red box) with number labels of the studied Ti grains and with ranges of tilt angles  $\Phi$ .

It is noteworthy that during the acquisition of the EBSD map of the electropolished Ti substrate of sample  $TiO_2^{ref}$ , amorphous carbon may have formed due to contamination of the surface with organic carbon species present in the microscope chamber and their subsequent decomposition by the highly energetic electron beam. The Raman spectrum of grain 5b is taken outside the zone of the EBSD map and shows a carbon signal very similar to the ones detected on grains 2 and 8 which are within the mapped zone (all three grains have tilt angles  $\Phi \leq \sim 15^\circ$ ). This observation shows that such contamination is negligible.

#### *Evaluation of Raman spectra of C/ $TiO_2$ :*

Figure S2a shows optical micrographs of the pristine anodic  $TiO_2$  and of the C/ $TiO_2$  film. Selected studied zones and the tilt angles of the corresponding Ti substrate grains are indicated. Figure S2b shows the background corrected spectral regions of the carbon signal from micro-Raman spectra of the C/ $TiO_2$  film, that were acquired on top of three substrate grains with different orientations (see 3D unit cells in the graph). For this sample, no EBSD map was acquired, so the azimuthal rotation  $\varphi_2$  about the c-axis of the hexagonal unit cell of Ti is unknown. Hence, the orange spectrum could also originate from a grain with different  $\varphi_2$ . A 4-peak Gaussian fit of the carbon signal was conducted and yields two peaks at  $\sim 1348$  and  $\sim 1600$   $cm^{-1}$  (D- and G-bands of carbon) and another two peaks at  $\sim 1235$  and  $\sim 1500$   $cm^{-1}$  (minor modulations associated with the D- and G-bands<sup>4,5</sup>, or adsorbed long-chain polyenes with varying number of double bonds that can form upon interaction of  $C_2H_2$  with  $TiO_2$ <sup>6-8</sup>). The intensity ratio  $I(D_1+D_2)/I(G_1+G_2)$ , where intensity refers to peak height, is about 0.7 - 0.8 for all substrate grains, which corresponds to an average cluster size of about 6 nm according to the Tuinstra-Koenig relation.<sup>4</sup>

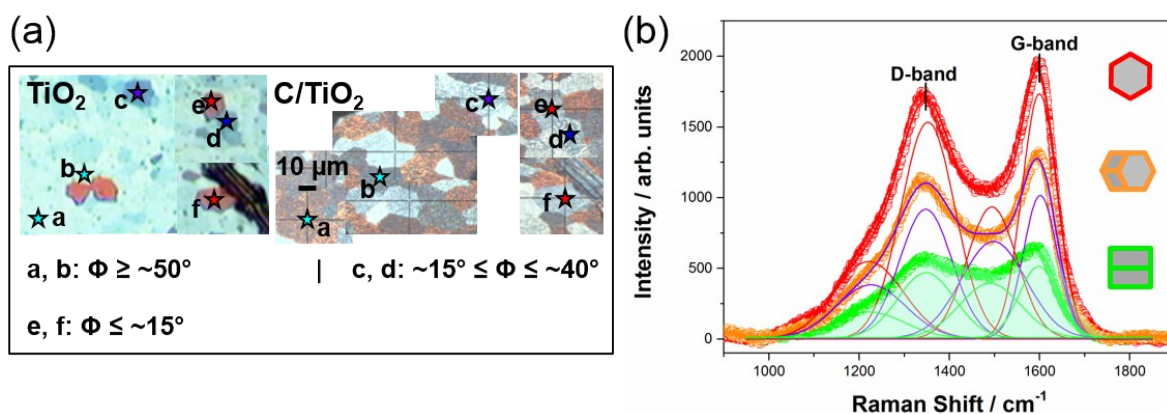


**Figure S2.** (a) Optical micrographs of the pristine anodic TiO<sub>2</sub> film and of the same film after thermal treatment with C<sub>2</sub>H<sub>2</sub> (C/TiO<sub>2</sub>). The estimated tilt angle ranges are given in the legend. (b) 4 peak Gaussian fits of the carbon signal of C/TiO<sub>2</sub> on top of Ti grains with different orientations.

### *X-ray photoelectron spectroscopy on C/TiO<sub>2</sub>:*

To identify the binding energies in the spectra from photoelectron micrographs (acquired with SPEM) that correspond to TiC or TiO species, a reference sample was prepared as follows: an anodic TiO<sub>2</sub> film was carbothermally treated with the same procedure that was employed to synthesize the herein studied C/TiO<sub>2</sub>, but with an annealing temperature of 650 °C instead of 550 °C. Figure S3 shows spectra from photoelectron micrographs of the C 1s and Ti 2p core-levels that were mapped with SPEM on the C/TiO<sub>2</sub> sample (550 °C) and on the reference sample (650 °C). Due to the higher carburization temperature, TiC and TiO species have formed in the reference sample and yield a photoelectron signal at 281.7 eV in the C 1s and at 454.9 eV in the Ti 2p spectrum.

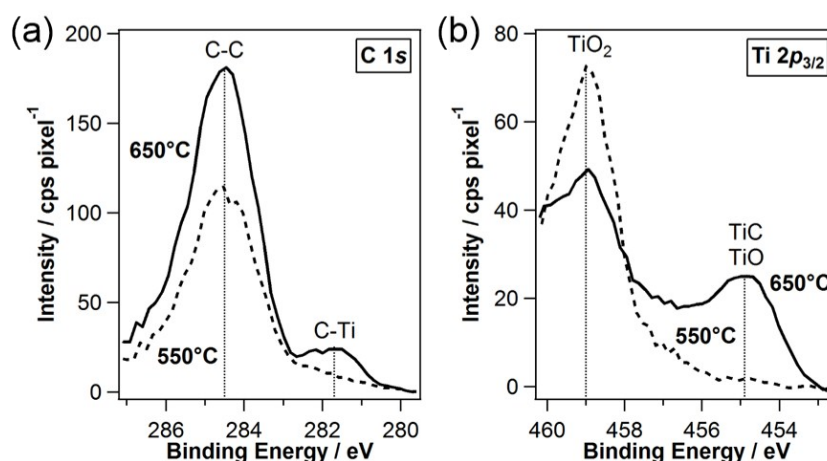


**Figure S3.** Spectra from photoelectron micrographs (obtained with SPEM) of the C 1s (a) and Ti 2p (b) core-level photoelectrons of C/TiO<sub>2</sub> (synthesized at 550 °C) and an anodic TiO<sub>2</sub> film that was carburized accordingly at 650 °C.

### *Effect of preferential orientation on the Raman response of thermally treated anodic TiO<sub>2</sub>:*

Due to their tetragonal structure, anatase and rutile TiO<sub>2</sub> are anisotropic Raman scatterers. Therefore, Raman bands of one symmetry are enhanced or suppressed compared to bands of other symmetry, depending on the orientation of the principal axis of the scatterer with respect to the polarization of the excitation laser beam.<sup>9–11</sup> In our case, the excitation laser was slightly polarized even without the use of a polarizer, hence variations in relative band intensities are

likely to occur when the sample is rotated about the surface normal (azimuthal rotation). To estimate this effect, oriented anatase crystals were studied as reference systems. Further they provided a standard for high crystallinity.

Raman measurements were performed with the same instrument and the same excitation laser (see Experimental section in main paper) on two natural anatase  $\text{TiO}_2$  crystals (SurfaceNet GmbH, Germany) with polished surfaces oriented parallel to the (001) and to the (100) plane, respectively, so that the incoming laser was perpendicular to one of these planes. A filter was used to reduce the laser intensity by a factor of 0.1; the Raman signal was acquired with a 100 x magnification in the spectral region from 80 to 800  $\text{cm}^{-1}$  during an acquisition time of 2 x 1 s. Two spectra of the (100) oriented anatase crystal were taken, where the crystal was positioned under the microscope with two azimuthal orientations differing from each other by about 90°. The same was done for selected grains of the  $\text{TiO}_2^{\text{ref}}$  and the C/ $\text{TiO}_2$  samples (applying the experimental settings described in the Experimental section of the main paper).

Figure S4 depicts the Raman response of polished (001) and (100) oriented anatase crystals. In Figure S4a, the  $E_g$  band at 143  $\text{cm}^{-1}$  is fitted with a Lorentzian function which yields a FWHM of 7  $\text{cm}^{-1}$ . Due to the rotational symmetry of the (001) plane around its surface normal (i.e. c-axis of anatase), an azimuthal rotation of the crystal underneath the microscope does not change the relative peak heights in the Raman spectrum (not shown). Depending on the azimuthal orientation of the (100) plane of anatase  $\text{TiO}_2$  with respect to the microscope, two different Raman spectra are obtained, where in one case, only the  $E_g$  bands are present. Furthermore, the relative intensity of the  $A_{1g}$  and  $B_{1g}$  bands (with respect to the intensity of the  $E_g$  bands) is higher for (001) than for (100) oriented anatase. This demonstrates the effect of the polarized laser light on the intensity of the Raman bands. Independent of crystal orientation with respect to the laser polarization (and the incident laser beam), all spectra are characterized by intense and sharp peaks, typical for extended single crystals.

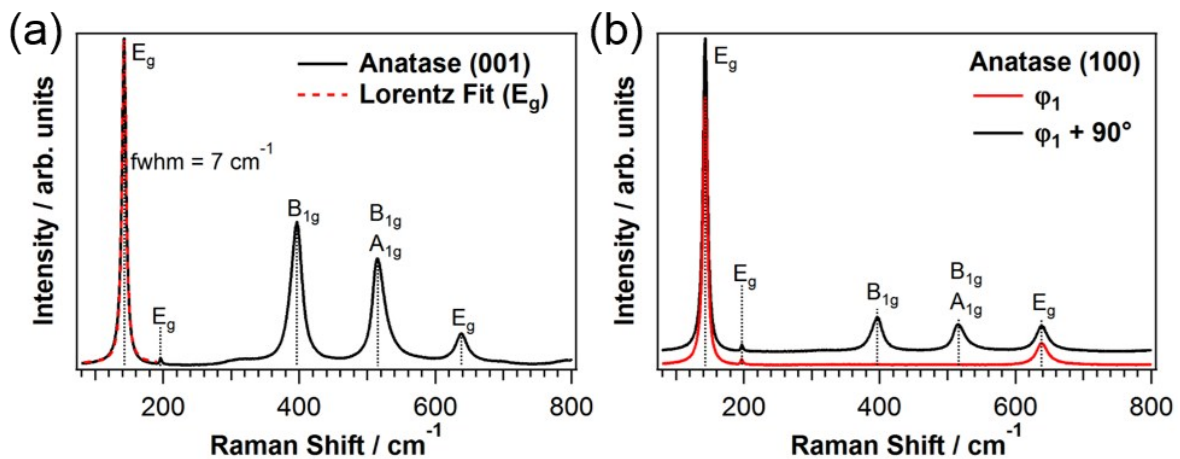


**Figure S4.** Raman spectra of natural anatase crystals with oriented polished surfaces. (a) Incident laser normal to (001) surface; red: Lorentzian peak fit. (b) Incident laser normal to (100) surface; spectra taken at two azimuthal orientations with respect to the microscope that differ by 90°. For clarity, the black spectrum is shifted upwards.

Figure S5 shows the Raman response of the  $\text{TiO}_2^{\text{ref}}$  (a) and of the C/ $\text{TiO}_2$  (b) film taken in two different azimuthal orientations relative to the Raman microscope. From Figure S5a (taking into account the reference spectra in Figure S4) it becomes clear that there is a preferential orientation of the anatase  $\text{TiO}_2$  phases in the  $\text{TiO}_2^{\text{ref}}$  film, which is more emphasized on top of Ti substrate grains with orientation of  $\sim(0001)$  (red curves in Figure S5a) compared to substrate grains with orientation of  $\sim\{2110\}$ . Yet the inset in Figure S5a shows that the intensity variation of the  $E_g$  band (at 143  $\text{cm}^{-1}$ ) due to preferential orientation can be neglected with respect to the effect of the Ti substrate grain orientation. The Raman response of the C/ $\text{TiO}_2$

film on top of three differently oriented substrate grains is depicted in Figure S5b. Also here, the spectral region associated with TiO<sub>2</sub> species is affected by the azimuthal orientation of the film relative to the laser polarization.

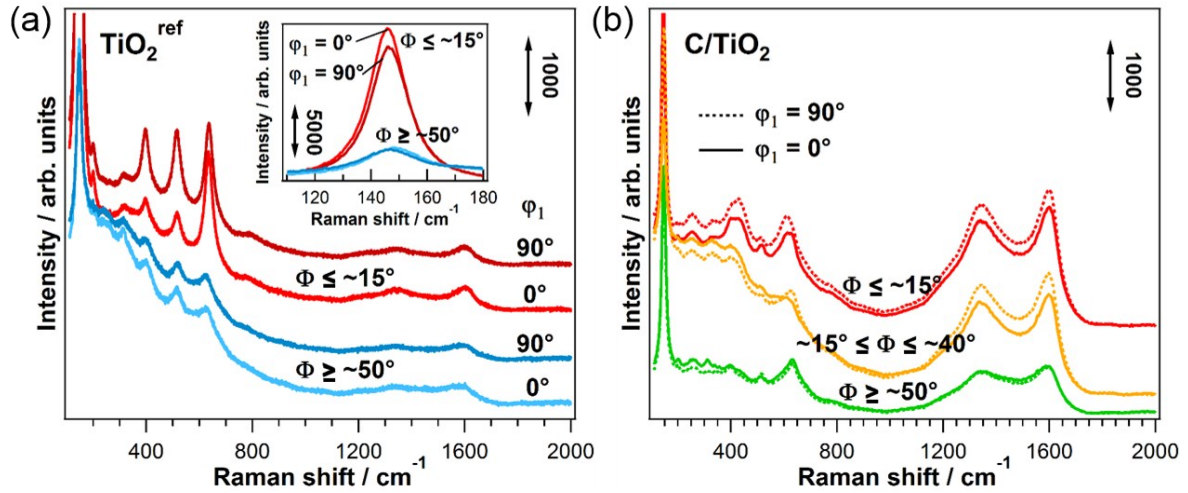


**Figure S5.** (a) Raman spectra of TiO<sub>2</sub><sup>ref</sup> sample for two different azimuthal orientations relative to the Raman microscope (0° and 90°). Red: film on a  $\sim$ Ti(0001) substrate grain; blue: film on a  $\sim$ Ti{*hki*0} substrate grain. (b) Raman spectra of C/TiO<sub>2</sub> for two different azimuthal orientations relative to the Raman microscope (0° and 90°). Red: film on a Ti substrate grain with tilt angle  $\Phi \leq \sim 15^\circ$  ( $\sim$ {0001}); yellow: film on a Ti substrate grain with tilt angle  $\sim 15^\circ \leq \Phi \leq \sim 40^\circ$ ; green: film on a substrate grain with tilt angle  $\Phi \geq \sim 50^\circ$  (and orientation of  $\sim$ {*hki*0}).

Even the Raman signal of carbon appears to be slightly influenced by the orientation of the sample surface with respect to the laser polarization. One might speculate that this is due to a combined effect of surface roughness (note that the intensity is not corrected for the real surface area) and anisotropic Raman scattering at disordered graphitic carbon;<sup>12,13</sup> the exact reason however cannot be clarified in the frame of this study. In any case, the pronounced variations in the intensities of the carbon spectrum with the substrate tilt angle  $\Phi$  cannot be explained by preferential orientation-effects.

#### *Evaluation of Raman spectra of TiO<sub>2</sub><sup>ref</sup>:*

Figure S6a shows a Lorentzian peak fit of the anatase E<sub>g</sub> band at  $\sim 143$  cm<sup>-1</sup> detected on the TiO<sub>2</sub><sup>ref</sup> film on top of substrate grains with three different orientations (see 3D unit cells extracted from EBSD). Also the anatase B<sub>1g</sub> band ( $\sim 396$  cm<sup>-1</sup>) and E<sub>g</sub> band ( $\sim 639$  cm<sup>-1</sup>) were fitted with Lorentzian line shapes (not shown). The amorphous background signal served as baseline. Therefore, the integrated peak area of the fitted anatase bands reflects the relative content of crystalline anatase TiO<sub>2</sub> without the amorphous contribution.

The carbon signals were fitted with four Gaussian peaks at  $\sim 1340$  and  $\sim 1600$  cm<sup>-1</sup> (D- and G-bands of ncg), 1227 and 1480 cm<sup>-1</sup> (minor modulations associated with the D- and G-bands<sup>4,5</sup>) as depicted in Figure S6b. The intensity ratio  $I(D_1+D_2)/I(G_1+G_2)$ , where intensity refers to peak height, is about 0.7 - 0.8 for all substrate grains, which corresponds to an average carbon cluster size of about 6 nm according to the Tuinstra-Koenig relation.<sup>4</sup>

As shown in Figure S6c for two selected substrate grain orientations, the total fraction of (amorphous and crystalline) TiO<sub>2</sub> in the film is estimated by integration of the overall Raman signal between 100 and 830 cm<sup>-1</sup>, covering the spectral range that contains all features associated with TiO<sub>2</sub>, after subtraction of a constant background.

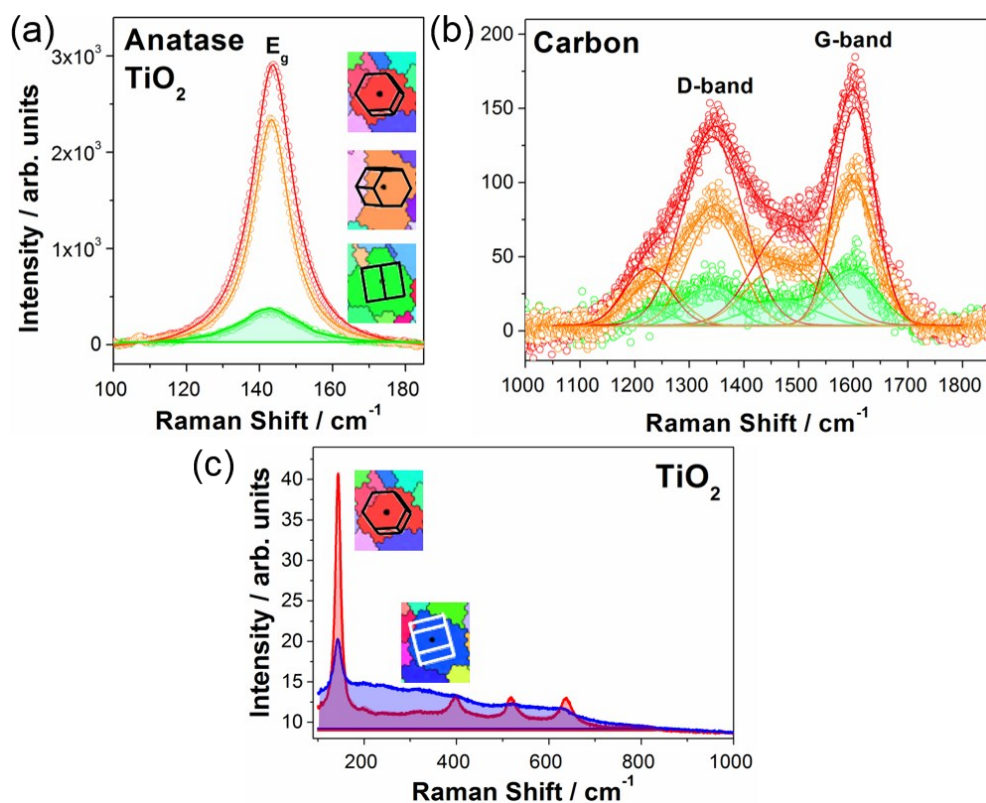


**Figure S6.** Analysis of selected Raman signals detected on TiO<sub>2</sub><sup>ref</sup> on top of substrate grains with the shown orientations. (a) Lorentz-fit of anatase E<sub>g</sub>-band at 143 cm<sup>-1</sup>. (b) 4-peak Gaussian fit of carbon signal. (c) Overall signal from thermally treated anodic TiO<sub>2</sub>; integrated areas are colored.

#### *Topography and roughness analysis of TiO<sub>2</sub><sup>ref</sup>:*

Contact-mode AFM was performed on the TiO<sub>2</sub><sup>ref</sup> sample with a Veeco Multimode 8 instrument (with a resolution of 512 pixels per line) to map the topography of individual grains and to determine the surface roughness. Analysis of the AFM micrographs was conducted with the NanoScope Analysis 1.5 software. First the images were pre-processed with plane fit and zero-order flattening procedures. On these images, roughness analysis was performed to gain information about the topographic surface area that is available for carbon deposition, when the sample is treated with C<sub>2</sub>H<sub>2</sub>. For that, image sections, the image root mean square height values (RMS) and roughness factors (RF = topographic area/projected area, where the topographic area is calculated by the sum of the area of three adjacent pixels) were extracted.

AFM analysis of the TiO<sub>2</sub><sup>ref</sup> film reveals a particulate or granular surface morphology (see images a-e in Figure S7). The roughness is affected by the tilt angle of the Ti substrate grains: high image contrast variations are detected on grains with  $\Phi = 12^\circ$ ,  $30^\circ$  and  $36^\circ$  (images a, b and c), while the TiO<sub>2</sub><sup>ref</sup> film is relatively smooth on grains with  $\Phi = 78^\circ$  (image d) and  $\Phi = 89^\circ$  (image e). On the TiO<sub>2</sub><sup>ref</sup> film of grain (c), the dimples that are caused by electropolishing and preserved during anodization are still visible. Cross-sections that are taken along the dashed lines in the micrographs are depicted in Figure S7f together with the 3D unit cells and tilt angles  $\Phi$ . It can be seen that relatively large protruding particulate features characterize the surface of the TiO<sub>2</sub><sup>ref</sup> film on the Ti substrate grains with tilt angles  $\Phi$  of  $12^\circ$ ,  $30^\circ$  and  $36^\circ$ . The width of the particulate shapes is of the order of 50 – 200 nm. In contrast, the TiO<sub>2</sub><sup>ref</sup> topography follows a relatively flat zigzag line with only weakly protruding particulate features on top of substrate grains with  $\Phi = 78^\circ$  and  $\Phi = 89^\circ$ . These observations show that upon crystallization, extensive structural reorganization has occurred on grains with substrate tilt angles  $\Phi \leq \sim 50^\circ$  which supports the presumption of an advanced anatase crystallization on these grains.

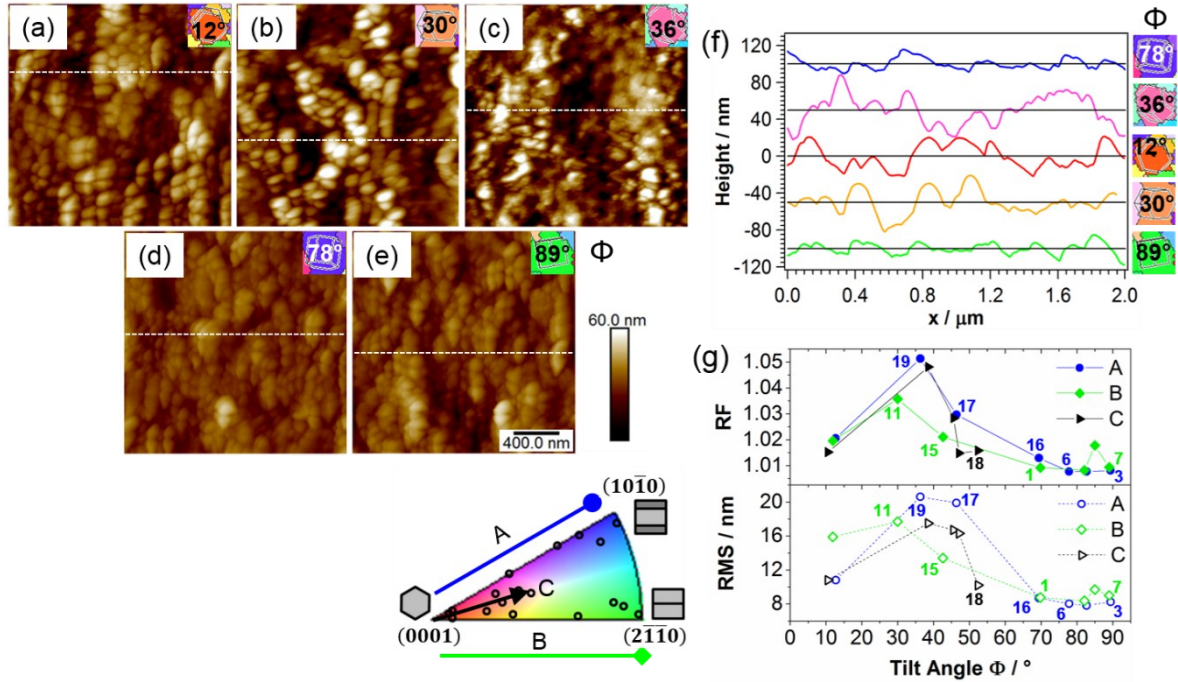


**Figure S7.**  $(2 \times 2) \mu\text{m}^2$  AFM micrographs of  $\text{TiO}_2^{\text{ref}}$ , taken on top of substrate grains with different crystallographic orientations (a – e). The insets show the corresponding 3D unit cells and tilt angles  $\Phi$ . Cross-sections in (f) are taken along the dashed lines in (a – e). (g) Dependence of the roughness factor (RF) and the root-mean-square (RMS) height on the tilt angle  $\Phi$  along three orientation paths in the standard triangle. The number labels belong to the grains in Figures 1 and S1.

To access the average topography of the entire oxide film on top of individual substrate grains, AFM-images of large scan size ( $15 \times 15 \mu\text{m}^2$ ) were acquired (not shown). Roughness analysis of the oxide film is performed on a zone inside the area of a substrate grain. Figure S7g depicts the obtained RMS (root mean square height) and RF (roughness factor) values of the analyzed  $\text{TiO}_2^{\text{ref}}$  zones versus the tilt angle  $\Phi$  of the Ti substrate grains along three different orientation paths (A, B, C) as indicated in the standard triangle. For all three orientation paths, the surface roughness varies with  $\Phi$ , but follows a similar trend, which shows that the tilt angle  $\Phi$  between c-axis and surface normal of the Ti substrate has an important influence on the topography of the overlying oxide film. Starting from mean values of  $\text{RF} = (1.018 \pm 0.003)$  and  $\text{RMS} = (12.5 \pm 2.9) \text{ nm}$  at  $\Phi \leq \sim 15^\circ$ , the roughness of the  $\text{TiO}_2^{\text{ref}}$  film passes through a maximum between  $\sim 30^\circ$  and  $\sim 40^\circ$  (grain 19:  $\text{RF} = 1.051$  and  $\text{RMS} = 20.6 \text{ nm}$ ) and drops to low values of  $\text{RF} = (1.010 \pm 0.004)$  and  $\text{RMS} = (8.6 \pm 2.9) \text{ nm}$  when the substrate grain orientation approaches tilt angles  $\Phi$  of  $70^\circ$  and higher. From the variation of RF with substrate tilt angle  $\Phi$  it becomes apparent that the differences in the film's surface roughness do not exceed 5 % (relative RF). This is by far too low to explain the observed differences in carbon content on the  $\text{TiO}_2^{\text{ref}}$  and C/ $\text{TiO}_2$  films when comparing zones on top of substrate grains with  $\Phi \leq \sim 15^\circ$  with zones on top of grains with  $\Phi \geq \sim 50^\circ$ .

#### *Analysis of Raman spectra of $\text{TiO}_2^{\text{ref}}$ :*

Additional analysis of the fits of the Raman spectra of  $\text{TiO}_2^{\text{ref}}$  is shown in Figure S8. In panel (a) the integrated areas (intensities) of the anatase  $E_g$  bands at  $\sim 143 \text{ cm}^{-1}$  and  $\sim 639 \text{ cm}^{-1}$  and the  $B_{1g}$  band at  $\sim 396 \text{ cm}^{-1}$  as well as the integrated areas of the prominent carbon D- and G-bands ( $\sim 1350$  and  $\sim 1600 \text{ cm}^{-1}$ ) are plotted versus the tilt angle  $\Phi$ .

Panels (b) and (c) depict the evolution of the Raman shift of the anatase  $B_{1g}$  band ( $\sim 396 \text{ cm}^{-1}$ ) and  $E_g$  band ( $\sim 639 \text{ cm}^{-1}$ ) with the tilt angle  $\Phi$  of the Ti substrate grains underneath the  $\text{TiO}_2^{\text{ref}}$  film. The orientations of the studied grains are indicated by spots in the standard triangle and

labeled with numbers (see also Figures 1 and S1). The intensity of all Raman peaks is increasing with decreasing substrate tilt angle, indicating an increasing grade of TiO<sub>2</sub> crystallinity (anatase) and a parallel increase in carbon content. The progressive blue-shift of the anatase B<sub>1g</sub> band towards the E<sub>g</sub> band of rutile at 447 cm<sup>-1</sup> and the parallel red-shift of the high frequency anatase E<sub>g</sub> band towards the A<sub>1g</sub> of rutile at 612 cm<sup>-1</sup> can be explained by an enhanced fraction of amorphous TiO<sub>2</sub> in the film, which exhibits Raman features at positions between the respective anatase and rutile bands (see Figure 5).

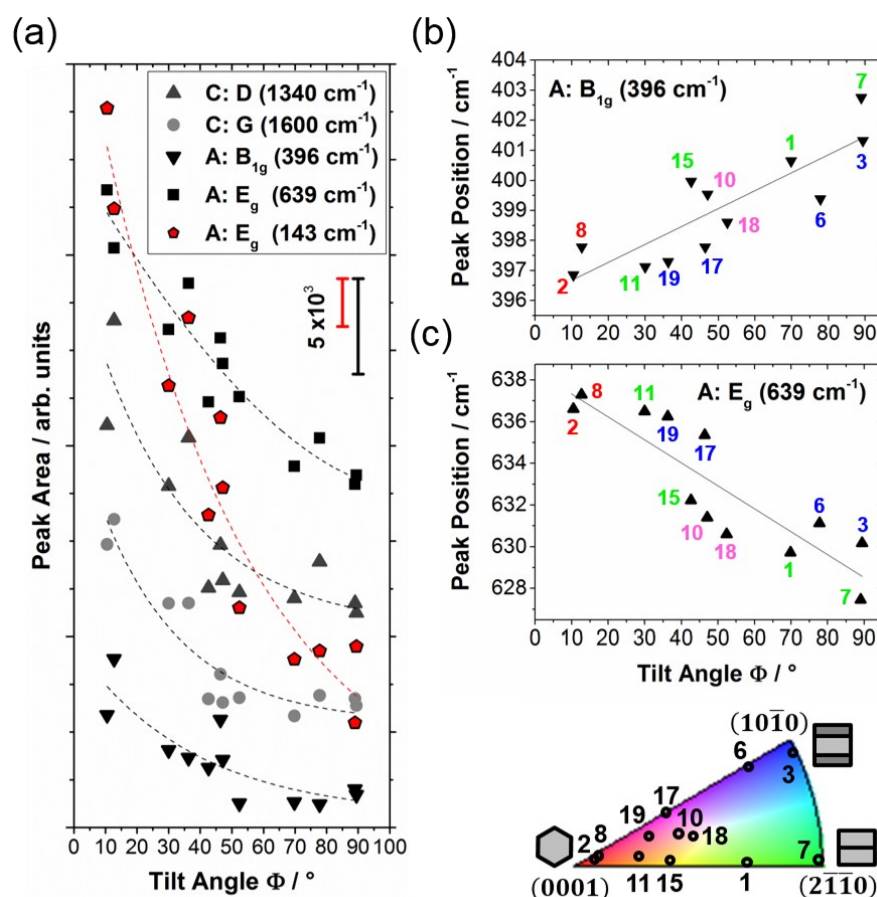


**Figure S8.** Evaluation of the fitted Raman-spectra of TiO<sub>2</sub><sup>ref</sup> on polycrystalline Ti. Integrated peak areas of five selected bands of the spectra (a) and band positions of two anatase bands (b, c) are plotted versus the tilt angle  $\Phi$  of the substrate grains. Mind the different scale bar for the anatase E<sub>g</sub> band at ~143 cm<sup>-1</sup> in panel (a). Solid lines are linear least squares fits, dotted lines serve as guide for the eye.

## References

- 1 D. L. Arsov, *Electrochim. Acta*, 1985, **30**, 1645.
- 2 J. Joseph and A. Gagnaire, *Thin Solid Films*, 1983, **103**, 257.
- 3 Y. Y. Wang, Z. H. Ni, Z. X. Shen, H. M. Wang and Y. H. Wu, *Appl. Phys. Lett.*, 2008, **92**, 043121.
- 4 A. C. Ferrari and J. Robertson, *Phys. Rev. B*, 2000, **61**, 95.

- 5 F. C. Tai, S. C. Lee, J. Chen, C. Wei and S. H. Chang, *J. Raman Spectrosc.*, 2009, **40**, 1055.
- 6 C. Tric, *J. Chem. Phys.*, 1969, **51**, 4778.
- 7 V. Rives-Arnau and N. Sheppard, *J. Chem. Soc. Faraday Trans. 1*, 1980, **76**, 394.
- 8 S. M. Jain, J. J. Biedrzycki, V. Maurino, A. Zecchina, L. Mino and G. Spoto, *J. Mater. Chem. A*, 2014, **2**, 12247.
- 9 S. P. S. Porto, P. A. Fleury and T. C. Damen, *Phys. Rev.*, 1967, **154**, 522.
- 10 T. Ohsaka, F. Izumi and Y. Fujiki, *J. Raman Spectrosc.*, 1978, **7**, 321.
- 11 W. Hayes and R. Loudon, *Scattering of light by crystals*, Wiley, New York, 1978.
- 12 S. Reich and C. Thomsen, *Philos. Trans. R. Soc. London A*, 2004, **362**, 2271.
- 13 A. C. Ferrari and D. M. Basko, *Nat. Nanotechnol.*, 2013, **8**, 235.